

Supporting Information

^{14}N - ^1H HMQC solid-state NMR as a powerful tool to study amorphous formulations – an exemplary study of paclitaxel loaded polymer micelles

*Marvin Grüne^a, Robert Luxenhofer^b, Dinu Iuga^c, Steven P. Brown^c, and Ann-Christin Pöppler^{*a}*

^a *Institute of Organic Chemistry, University of Würzburg, Am Hubland, 97074 Würzburg, Germany*

^b *Lehrstuhl für Chemische Technologie der Materialsynthese, University of Würzburg, Röntgenring 11, 97070 Würzburg, Germany*

^c *Department of Physics, University of Warwick, Coventry, CV4 7AL, United Kingdom*

Supporting Information

Content:

- SI 1. Calculation of the second-order isotropic quadrupolar shift
- SI 2. Pulse Sequence
- SI 3. Preparation of the Paclitaxel (PTX)-Polymer Formulations and amorphous Paclitaxel
- SI 4. Chemical shifts of the Polymer (POL) in solution
- SI 5. NMR characterization of PTX in solution
- SI 6. ^1H NMR spectra of unloaded and loaded polymer micelles in D_2O recorded with a cryoprobe
- SI 7. PXRD measurements
- SI 8. Solid-state NMR - ^{14}N - ^1H HMQC of the Dipeptide β -Asp-Ala
- SI 9. ^{14}N - ^1H HMQC of amorphous PTX
- SI 10. Crystal structure of PTX
- SI 11. References

SI 1: Calculation of the second-order isotropic quadrupolar shift¹

For a quadrupolar nucleus, in addition to the isotropic chemical shift, there is an isotropic second-order quadrupolar shift: For the $(m, m-1)$ transition, this is given in ppm as:^{2,3}

$$\delta_{iso}^Q = \left\{ -\frac{\frac{3}{40} \left(\frac{P_Q}{\nu_0}\right)^2 [I(I+1) - 9m(m-1) - 3]}{[I^2(2I-1)^2]} \right\} \times 10^6$$

where ν_0 is the Larmor frequency in Hz and the quadrupolar product, P_Q , is defined as:

$$P_Q = C_Q \sqrt{\left[1 + \frac{\eta_Q^2}{3}\right]}$$

The quadrupolar coupling constant, C_Q , and asymmetry, η_Q , depend on the principal components of the electric field gradient tensor that are ordered such that: $|V_{ZZ}| \geq |V_{YY}| \geq |V_{XX}|$. Specifically, the quadrupolar coupling constant, C_Q , (in units of Hz) is given by:

$$C_Q = \frac{V_{ZZ}eQ}{h} = \frac{e^2qQ}{h}$$

where Q is the nuclear quadrupole moment and q is the electric field gradient, and e and h are the charge of an electron and Planck's constant, respectively. The asymmetry is defined as:

$$\eta_Q = \frac{V_{XX} - V_{YY}}{V_{ZZ}}$$

SI 2: Pulse Sequence

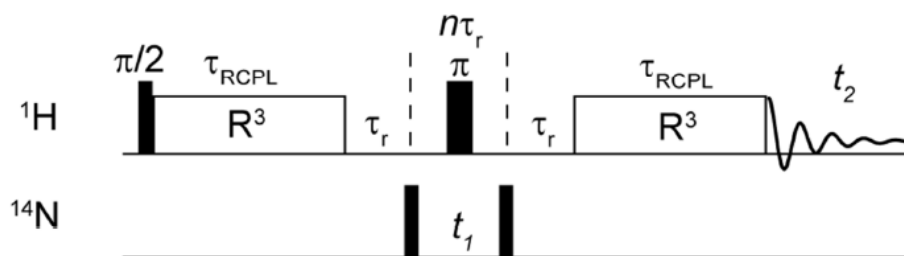


Figure S1: ^{14}N - ^1H HMQC pulse sequence using the R^3 rotary resonance sequence to recouple heteronuclear dipolar couplings.¹

All NMR data of this manuscript is uploaded at the Warwick Research Archive Portal (WRAP). Thus, the full compiled pulse sequence as used for the experiments is available as a text document. For further information on practical aspects of ^{14}N - ^1H HMQC experiments the reader is also referred to chapter 2 in the book "Modern Methods in Solid-state NMR: A Practitioner's Guide".⁴

SI 3: Preparation of the Paclitaxel (PTX)-Polymer Formulations and amorphous Paclitaxel

The three formulations with different drug load were prepared according to existing preparation protocols.⁵ Throughout this manuscript, the formulations are referred to as POL-2-PTX, POL-4-PTX and POL-9-PTX. The numbers 2,4 and 9 describe the polymer to drug ratio (by weight) of the formulation. The different concentrations used for preparation and the median hydrodynamic radius (literature data) of the micelles are listed in Table S1.

Formulation	Ratio (POL/PTX) (w/w)	% wt	Concentration POL (g/L)	Solubilized concentration PTX (g/L)	Median Hydrodynamic Radius (R _h) ⁶
P2-2-PTX	10:2	17 %	10 g/L	2 g/L	6 nm
P2-4-PTX	10:4	29 %	10 g/L	4 g/L	8 nm
P2-9-PTX	10:9	47 %	10 g/L	9 g/L	11 nm

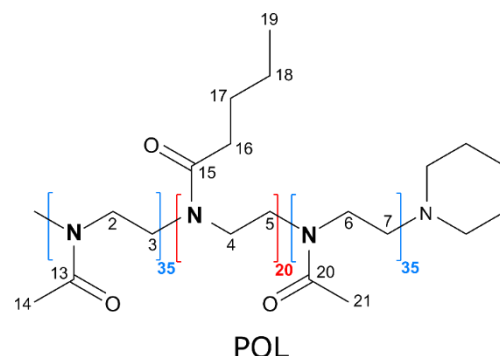
All three formulations were produced by combining the appropriate amount of ethanolic polymer and PTX solutions. Ethanol was then evaporated, the resulting thin film dissolved in H₂O and lyophilized to give a white powder.

Lyophilization was also used to prepare amorphous PTX. PXRD data shown in figure S4 confirmed the amorphicity.

SI 4: Chemical shifts of the Polymer (POL) in solution

Assignment of the ^1H and ^{13}C chemical shifts in solution, was carried out based on a standard set of 1D and 2D NMR experiments including ^1H - ^1H COSY, ^1H - ^{13}C HSQC and HMBC experiments. In CDCl_3 , the individual polymer strands do not self-assemble, while in D_2O the amphiphilic triblock copolymer forms spherical and wormlike micellar structures.

C	CDCl_3 [ppm]	D_2O [ppm]	H of C	CDCl_3 [ppm]	D_2O [ppm]
2,3,6,7	48.1- 43.7	46.3, 44.2,	2,3,6,7	3.49- 3.25	3.51-3.47
4,5		47.2, 46.7			4, 5
13/20	171.5, 170.9	174.3			
14/21	21.3	20.2	14/21	2.14- 2.08	2.09-2.02
15	174.0, 173.4	Not visible			
16	32.6	32.3	16	2.37- 2.31,	2.36-2.26
17	27.4	27.3	17	1.61- 1.53	1.51-1.47
18	22.7	22.0	18	1.39- 1.30	1.34-1.27
19	14.1	13.3	19	0.93- 0.90	0.89-0.85



Further discussion related to Figure 2b in the main manuscript:

- Assignment:** The ^{13}C chemical shifts in the solid state agreed well with the chemical shifts observed in solution and also with a structurally similar polymer with a propyl instead of a butyl sidechain (ref. 18). For the ^1H chemical shift assignment, NMR data in solution alongside ^1H - ^1H NOESY-like solid-state NMR spectra in the solid state were used (Figure S2). At lowest mixing time (Figure S2a, 20 ms), the end group of the propyl chain (Me, 19) is in contact with the adjacent signal (17,18) and to a lesser extent with the next signal at higher ppm, while this signal (14,16,21) is the only one showing cross-peaks to the backbone of the polymer (arrow, 2-7). With increasing mixing time, first an additional signal between the CH_2 groups of the butyl chain (17,18) and the backbone (Figure S2b) and upon further increase finally to the Bu-CH_3 group (Figure S2c) is observed.
- Discussion of the HMQC signals:** Another interesting feature is the broadening of the backbone resonance upon increasing the mixing time. The backbone is the most rigid area of the triblock copolymer. Although the recoupling times in the HMQC are on a much shorter timescale, signal loss due to relaxation could be a possibility for the absence of $\text{N}\cdots\text{H}$ contacts to the backbone protons. Furthermore, even without guest molecules, the polymers form micellar nanoparticles. In these self-assembled systems, proximity between the butyl chain of one polymer block with a nitrogen atom

from a more distant repeating unit or a different polymer chain is more likely than a backfolding of the butyl chain to generate contact to the directly bound nitrogen.

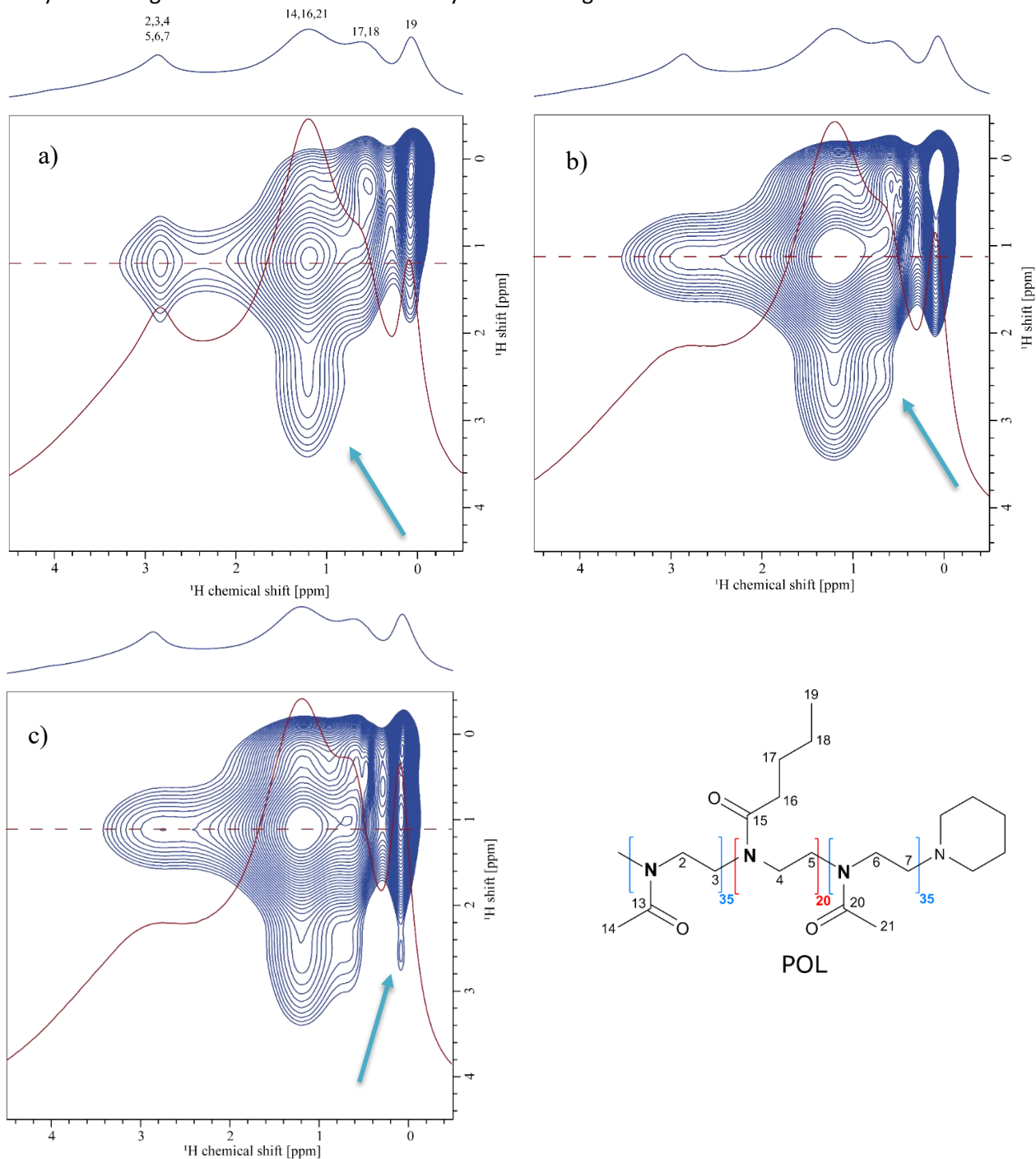


Figure S2: ^1H - ^1H NOESY-like solid-state NMR spectrum recorded at 20 T and a MAS frequency of 60 kHz for POL (heated above T_g prior to the measurement), using a mixing time of a) $\tau_{mix} = 20$ ms, b) $\tau_{mix} = 50$ ms and $\tau_{mix} = 100$ ms. 178 t_1 FIDs increments were acquired for each experiment using a recycle delay of 1.8 s, each with 32 co-added transients. The base contour level is at 22% (a) and 40% (b, c) of the maximum peak height. The corresponding ^1H one-pulse MAS NMR spectrum is shown as external projection.

SI 5: NMR characterization of PTX in solution

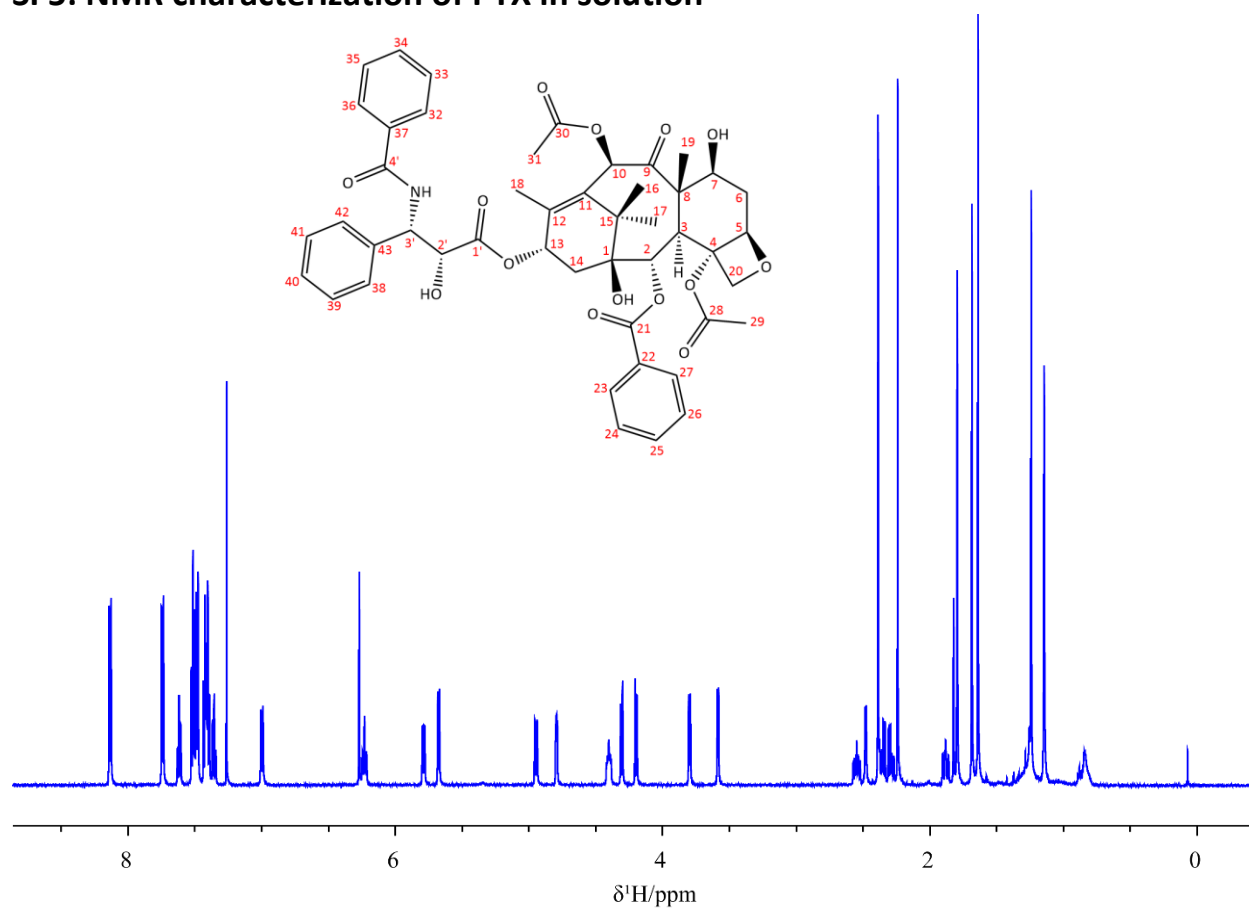


Figure S3a: ¹H NMR spectrum of pure PTX (as received) in CDCl₃, recorded with 16 scans and a recycle delay of 5.8 s. The dataset was recorded on a Bruker Avance III HD 14.1 T spectrometer equipped with a 5 mm BBFO BB/19F-1H/D probe at 295.2 K. The temperature was calibrated using 4% MeOH in MeOD.

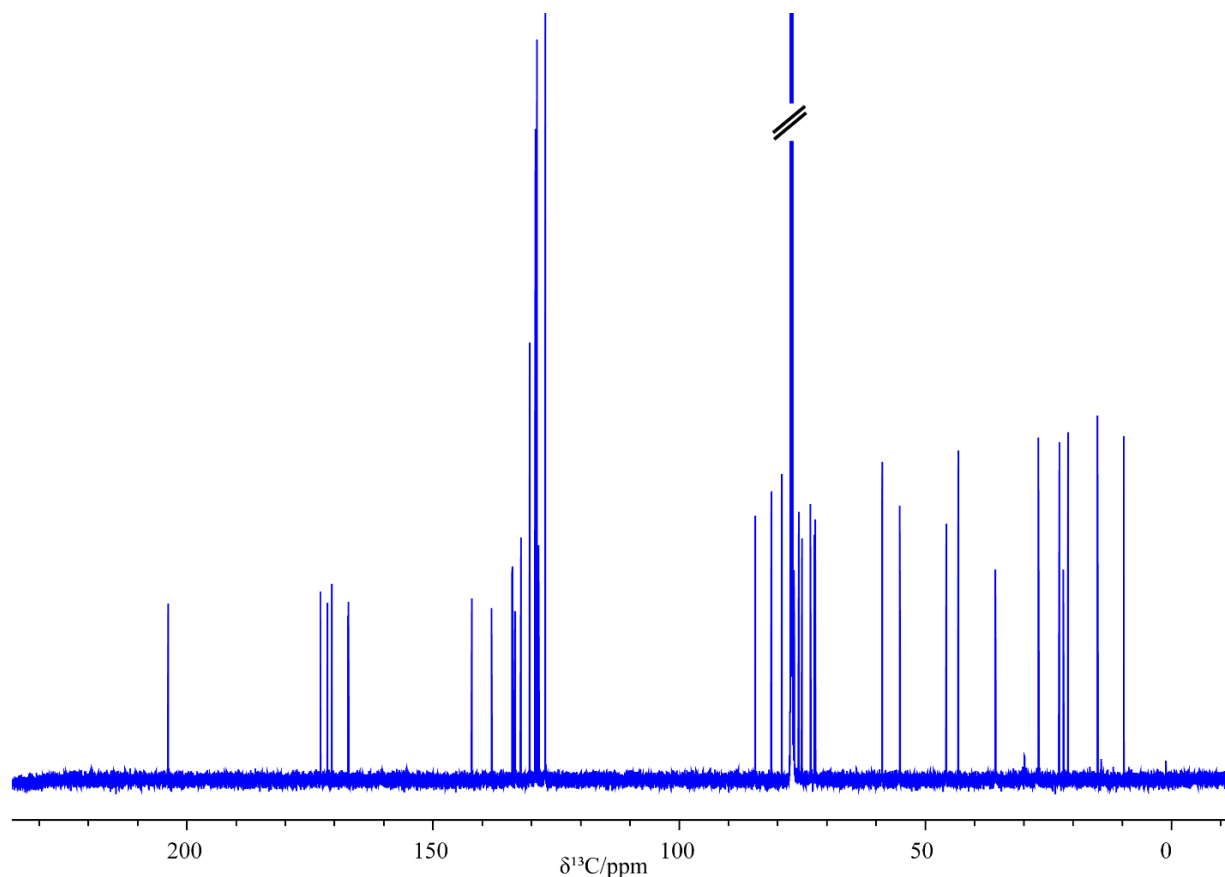


Figure S3b: $^{13}\text{C}/(^1\text{H})$ NMR spectrum of pure PTX (as received) in CDCl_3 , recorded with 8192 scans and a recycle delay of 2.8 s. The dataset was recorded on a Bruker Avance III HD 14.1 T spectrometer equipped with a 5 mm BBFO BB/19F-1H/D probe at 295.2 K. The temperature was calibrated using 4% MeOH in MeOD.

For clarity, the following ^1H NMR assignment for PTX uses the carbon numbering scheme from above in the way that, for example, C25, indicates the proton bound to carbon C25.

^1H -NMR (600.4 MHz, CDCl_3): δ = 8.13 (m, 2 H, CH, C23/27 (o)), 7.74 (m, 2 H, CH, C33/35 (m)), 7.61 (m, 1 H, CH, C25 (p)), 7.52-7.47 (m, 5 H, CH, C24/26 (m), C34(p), C38/42 (o)), 7.43-7.40 (m, 4 H, CH, C32/36 (o), C39/41 (m)), 7.35 (m, 1 H, CH, C40 (p)), 6.99 (d, 1 H, NH, $^3J_{\text{C}3'-\text{NH}}$ = 8.9 Hz, NH), 6.27 (s, 1 H, CH, C10), 6.23 (m, 1 H, CH, C13), 5.79 (dd, 1 H, CH, $^3J_{\text{C}2'-\text{C}3'}$ = 2.6 Hz, $^3J_{\text{C}3'-\text{NH}}$ = 8.9 Hz, C3'), 5.67 (d, 1 H, CH, $^3J_{\text{C}2-\text{C}3}$ = 7.0 Hz, C2), 4.95 (dd, 1 H, CH, $^3J_{\text{C}5-\text{C}6a}$ = 1.9 Hz, $^3J_{\text{C}5-\text{C}6e}$ = 9.6 Hz, C5), 4.79 (d, 1 H, CH, $^3J_{\text{C}2'-\text{C}3'}$ = 2.7 Hz, C2'), 4.40 (dd, 1 H, CH, $^3J_{\text{C}7-\text{C}6a}$ = 10.9 Hz, $^3J_{\text{C}7-\text{C}6e}$ = 6.8 Hz, C7), 4.31 (d, 1 H, CH_2 , $^2J_{\text{C}20-\text{C}20}$ = 8.5 Hz, C20), 4.19 (d, 1 H, CH_2 , $^2J_{\text{C}20-\text{C}20}$ = 8.5 Hz, C20), 3.80 (d, 1 H, CH, $^3J_{\text{C}2-\text{C}3}$ = 7.0 Hz, C3), 3.57 (s, 3 H, CH_3 , C2'-OH), 2.59-2.48 (ddd, 1 H, CH, $^2J_{\text{C}6a-\text{C}6e}$ = 15.0 Hz, $^3J_{\text{C}5-\text{C}6e}$ = 9.7 Hz, $^3J_{\text{C}7-\text{C}6e}$ = 6.7 Hz, C6e), 2.47 (s, 1 H, OH, C7-OH), 2.39 (s, 3 H, CH_3 , C29), 2.35 (dd, 1 H, CH, $^2J_{\text{C}14a-\text{C}14e}$ = 15.4 Hz, $^3J_{\text{C}13-\text{C}14e}$ = 9.0 Hz, C14e), 2.28 (dd, 1 H, CH, $^2J_{\text{C}14a-\text{C}14e}$ = 15.4 Hz, $^3J_{\text{C}13-\text{C}14a}$ = 9.0 Hz, C14a), 2.24 (s, 3 H, CH_3 , C31), 1.92-1.85 (ddd, 1 H, CH, $^2J_{\text{C}6a-\text{C}6e}$ = 14.7 Hz, $^3J_{\text{C}5-\text{C}6a}$ = 2.3 Hz, $^3J_{\text{C}7-\text{C}6a}$ = 11.0 Hz, C6a), 1.79 (d, 3 H, CH_3 , $^4J_{\text{C}18-\text{C}13}$ = 1.1 Hz, C18), 1.68 (s, 3 H, CH_3 , C19), 1.24 (s, 3 H, CH_3 , C16), 1.14 (s, 3 H, CH_3 , C17) ppm.

¹³C-NMR (100.6 MHz, CDCl₃): δ = 203.8 (1 C, C_q, C9), 172.9 (1 C, C_q, C1'), 171.4 (1 C, C_q, C30), 170.5 (1 C, C_q, C28), 167.2 (1 C, C_q, C21), 167.2 (1 C, C_q, C4'), 142.1 (1 C, C_q, C12), 138.1 (2 C, C_q, C37/43), 133.9 (1 C, C_q, C22), 133.7 (1 C, CH, C25 (p)), 133.3 (1 C, C_q, C11), 132.1 (1 C, CH, C34 (p)), 130.4 (2 C, CH, C23/27 (o)), 129.3 (2 C, CH, C38/42 (o)), 129.2 (1 C, CH, C39/41 (m)), 128.88 (1 C, CH, C39/41 (m)), 128.86 (4 C, CH, C24/26 (m), C32/36 (o)), 128.5 (1 C, CH, C40 (p)), 127.2 (2 C, CH, C33/35 (m)), 127.2 (2 C, CH, C38/42 (o)), 84.6 (1 C, CH, C5), 81.3 (1 C, C_q, C4), 79.2 (1 C, C_q, C1), 76.7 (1 C, CH₂, C20), 75.7 (1 C, CH, C10), 75.1 (1 C, CH, C2), 73.3 (1 C, CH, C2'), 72.5 (1 C, CH, C13), 72.3 (1 C, CH, C7), 58.8 (1 C, C_q, C8), 55.2 (1 C, CH, C3'), 45.7 (1 C, CH, C3), 43.3 (1 C, C_q, C15), 35.8 (1 C, CH₂, C14), 35.7 (1 C, CH₂, C6), 27.0 (1 C, CH₃, C16a), 22.8 (1 C, CH₃, C29), 22.0 (1 C, CH₃, C17e), 21.0 (1 C, CH₃, C31), 15.0 (1 C, CH₃, C18), 9.7 (1 C, CH₃, C19) ppm.

SI 6: ¹H NMR spectra of unloaded and loaded polymer micelles in D₂O recorded with a cryoprobe

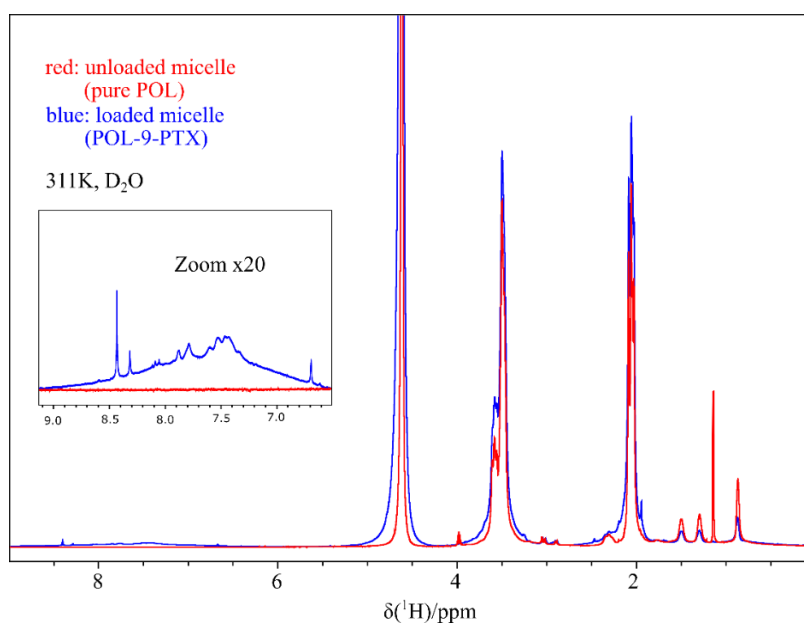


Figure S4a: ¹H NMR spectra of pure POL (red), forming an unloaded micelle in D₂O, and of a loaded micelle (POL-9-PTX) in D₂O (blue), recorded with a recycle delay of 5.8 s with 64 and 400 co-added transients, respectively. Both datasets were measured on a 14.1 T Bruker Avance III HD spectrometer equipped with a 5 mm ¹³C/¹H cryoprobe at 311 K. The temperature was calibrated using 80% ethylene glycol in DMSO-d₆.

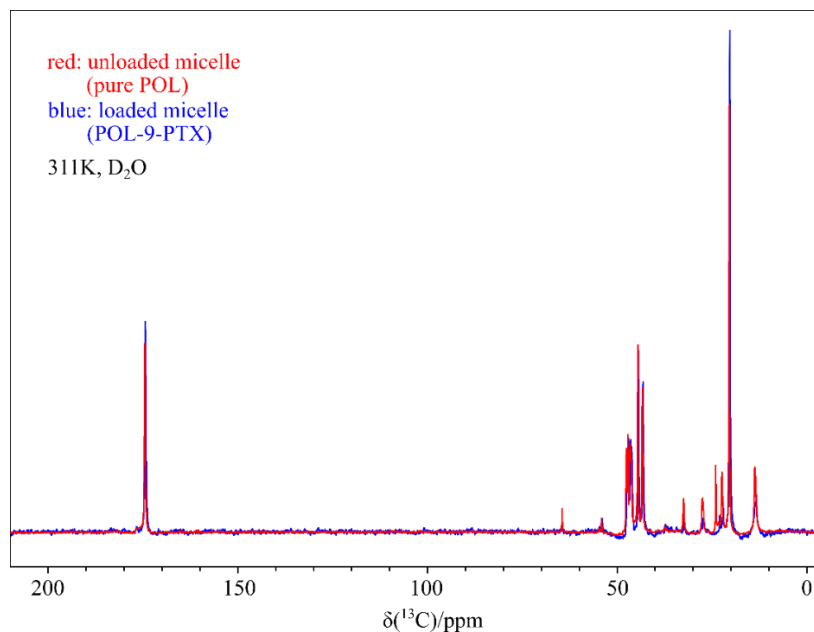


Figure S4b: Proton decoupled ^{13}C NMR spectra of pure POL (red), forming an unloaded micelle in D_2O , recorded with 26624 co-added transients and of the loaded micelle (POL-9-PTX) in D_2O (blue), recorded with 26562 co-added transients. Both datasets were measured for a recycle delay of 2.8 s on a 14.1 T Bruker Avance III HD spectrometer equipped with a 5 mm $^{13}\text{C}/^1\text{H}$ cryoprobe at 311 K. The temperature was calibrated using 80% ethylene glycol in DMSO-d_6 .

Figure S3a and S3b show ^1H and ^{13}C NMR spectra of unloaded as well as of PTX-loaded polymer micelles. All spectra were recorded at 311K to mimic body temperature conditions in blood circulation. In Figure S3a, the aromatic region of the protons (enlarged region) is of particular interest. This region only contains PTX signals. Due to the low signal intensity and the broad line widths, it is challenging to investigate the incorporation of PTX into the micelles via ^1H NMR data in solution. Figure S3b demonstrates that even after recording more than 26000 scans for a ^{13}C NMR experiment in solution using a cryoprobe at 14.1 T, no visible signals of the PTX appear between 70 and 150 ppm. In this region, no POL peaks would be expected.

SI 7: PXRD measurements

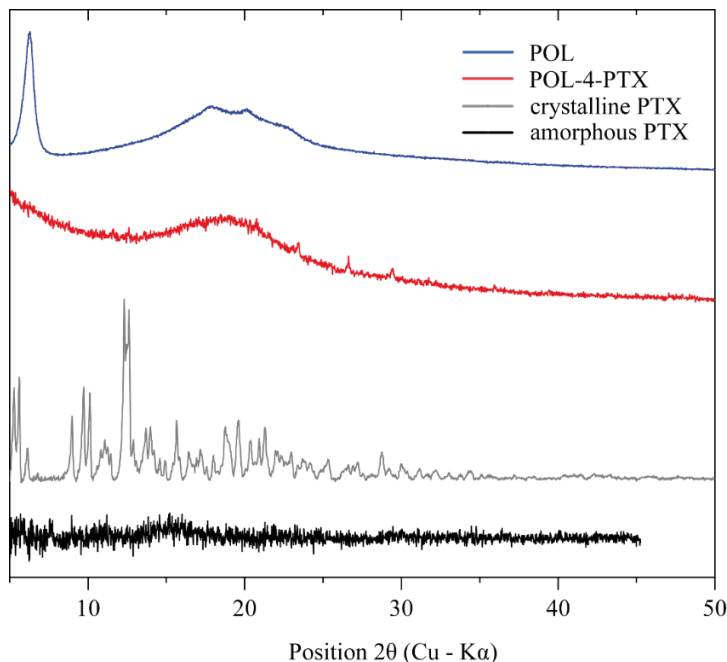


Figure S5: PXRD data of POL (blue), an exemplary formulation POL-4-PTX (red), crystalline PTX (grey) and amorphous PTX (black). Powder diffraction data was recorded on a Bruker Discover D8 powder diffractometer (Karlsruhe, Germany) using Cu K α radiation (unsplit K α 1+K α 2 doublet, mean wavelength λ = 154.19 pm) at a power of 40 kV and 40 mA, a focusing Goebel mirror, and a 2.5° axial Soller slit. The scattered X-ray beam went through a receiving slit (3.3°). Detection was achieved with a LynxEye-1D-Detector (Bruker AXS) using the full detector range of 192 channels. Measurements were done in reflection geometry in coupled two theta/theta mode with a step size of 0.025° in the range 2 θ of 5° to 45° (black) or 50° (blue, red, grey). The software package DIFFRAC.Suite (V2 2.2.690, BrukerAXS 2009–2011, Karlsruhe, Germany) was used for data collection. The diffraction data was subsequently converted into ASCII format and further handled with Origin (OriginLab, Massachusetts, USA).

POL-4-PTX mainly shows the expected amorphous character. The two peaks between 25-30° correspond to PTX, which still forms some small ordered phases within the formulation. Different PTX batches of the same company yielded slightly different phases, which is further discussed in SI 8.

SI 8: Solid-state NMR - ^{14}N - ^1H HMQC of the Dipeptide β -Asp-Ala

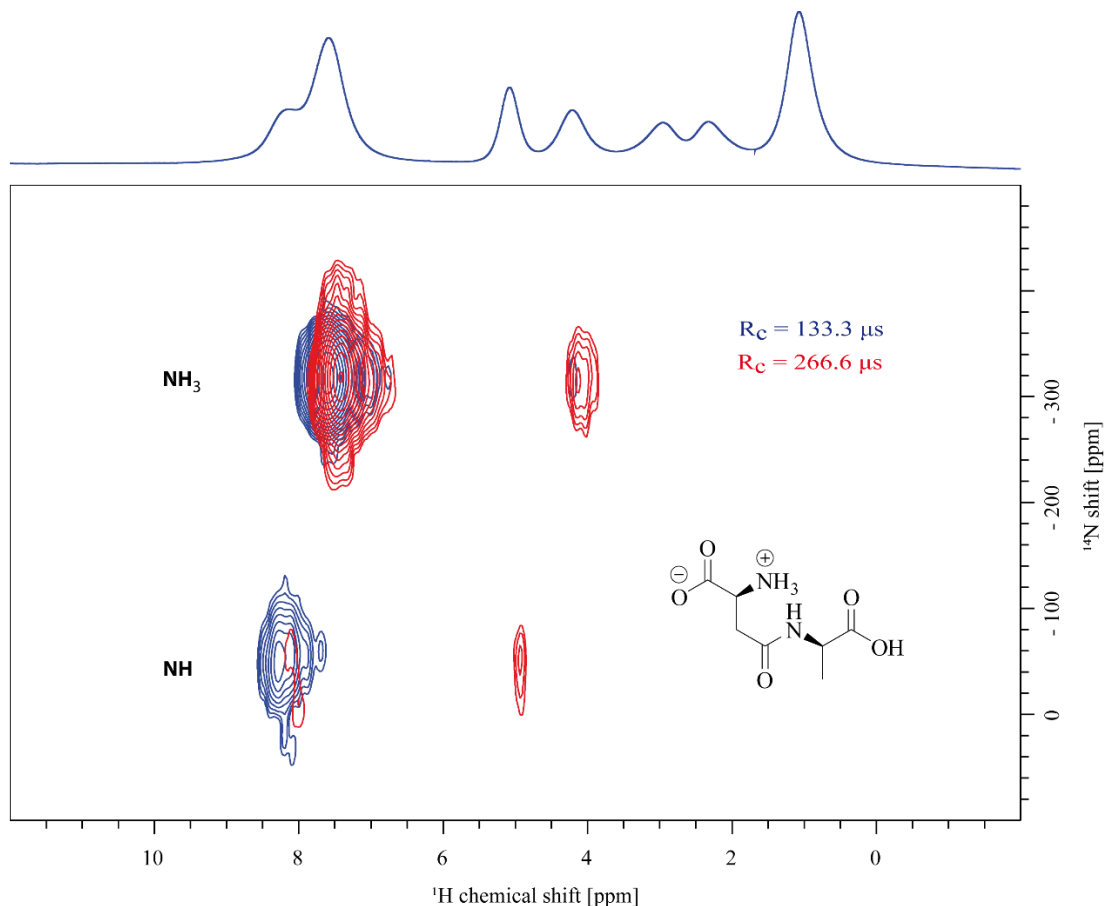


Figure S6: ^{14}N - ^1H HMQC spectra recorded at 20 T and a MAS frequency of 60 kHz for the dipeptide β -AspAla using a recoupling time (τ_{RCL}) of $R_c = 133 \mu\text{s}$ (blue) and $R_c = 266 \mu\text{s}$ (red). 64 t_1 FIDs increments were acquired, each with 16 co-added transients and a recycle delay of 1.0 s. A ^1H one-pulse MAS NMR spectrum of β -AspAla is shown as external projection.

Figure S6 illustrates ^{14}N - ^1H HMQC test measurements of the dipeptide β -Asp-Ala. By varying the recoupling time, it is possible to observe increasingly longer-range through-space proximities, e.g. longer recoupling times probing longer range intra- and intermolecular $\text{N}\cdots\text{H}$ proximities (see further investigations of this by Tatton et. al.¹). Comparison of the red and blue spectra reveals that the increase in recoupling time yields additional $\text{N}\cdots\text{H}$ contacts and that the signal intensity of the directly bound NH decreases with increasing recoupling time.

SI 9: ^{14}N - ^1H HMQC of amorphous PTX

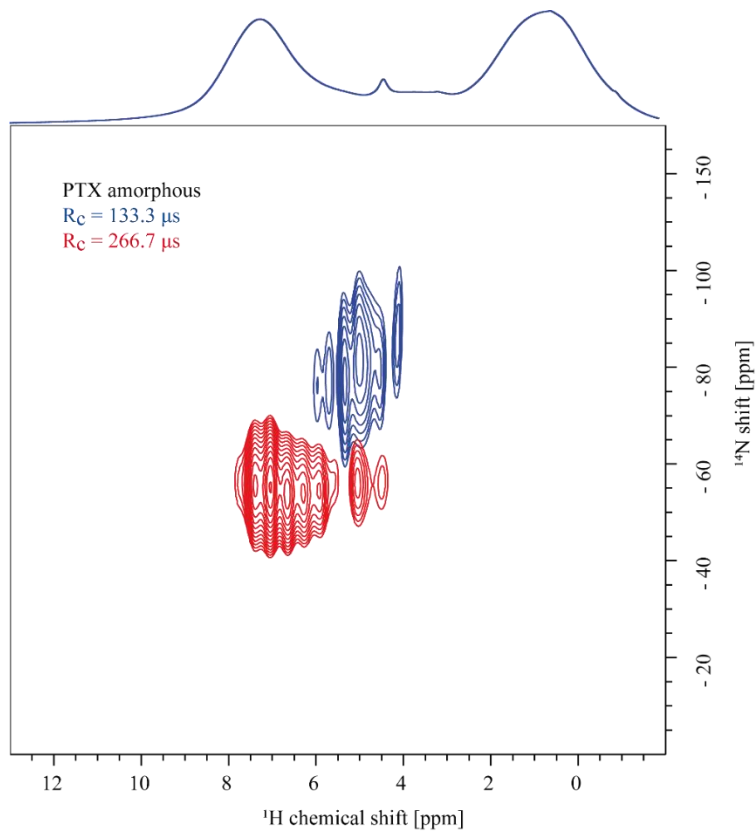


Figure S7: ^{14}N - ^1H HMQC spectra recorded at 20 T and a MAS frequency of 60 kHz for amorphous paclitaxel using a recoupling time (τ_{RCPL}) of blue: $R_c = 133.3 \mu\text{s}$, red: $R_c = 266.7 \mu\text{s}$. 34 t_1 FIDs increments were acquired using a recycle delay of 2.0 s, each with 240 co-added transients resulting in an overall experimental time of 4 h 40 min. The corresponding ^1H one-pulse MAS NMR spectrum is shown as external projection.

SI 10: Crystal structure of PTX

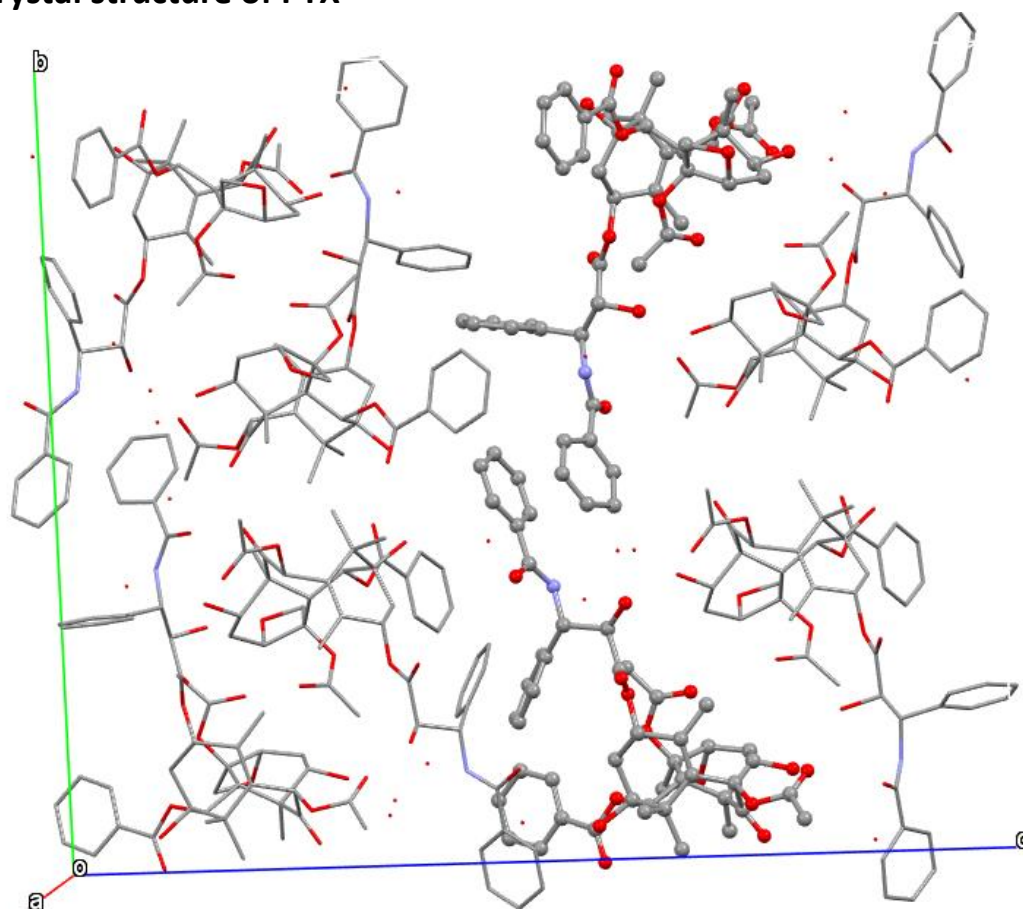


Figure S8: Unit cell of PTX. Hydrate structure of PTX published by Vella-Zarb et al.⁷ with the CCDC name RIGKUP and CCDC number 912149. This structure contains two molecules of PTX in the asymmetric unit and six additional water molecules. The original structure was obtained by single-crystal synchrotron XRD data at a temperature of 120.15 K. The two individual PTX molecules in the asymmetric unit are highlighted above.

SI 11: References

1. Tatton AS, Bradley JP, Iuga D, Brown SP. Z Phys Chem. 2012;**226(11-12)**,1187-204.
2. Gan Z, Amoureux JP, Trebosc J. Chem Phys Lett. 2007;**435(1-3)**,163-9.
3. Samoson A. Chem Phys Lett. 1985;**119(1)**,29-32.
4. Brown SP. Chapter 2, High-resolution ^1H 2D Magic-angle Spinning Techniques for Organic Solids. Modern Methods in Solid-state NMR: A Practitioner's Guide: The Royal Society of Chemistry; 2018. p. 39-74.
5. Luxenhofer R, Schulz A, Roques C, Li S, Bronich TK, Batrakova EV, et al. Biomaterials. 2010;**31(18)**,4972-9.
6. Schulz A, Jaksch S, Schubel R, Wegener E, Di Z, Han Y, et al. ACS nano. 2014;**8(3)**,2686-96.
7. Vella-Zarb L, Baisch U, Dinnebier RE. J Pharm Sci. 2013;**102(2)**,674-83.